Supplemental Information

Efficient clearance of periodontitis pathogens by *S. gordonii* membrane-coated H_2O_2 self-supplied nanocomposites in a "Jenga" style

Qinghua Cao,[a] Xiang Xiao,[a] Chengcheng Tao,[a] Rui Shi,*[a,b] Rui Lv,[a] Ruochen Guo,[a] Xinyi Li,[a] Baiyan Sui,[c] Xin Liu,[c] Jian Liu,*[a]

a. Institute of Functional Nano & Soft Materials (FUNSOM), Jiangsu Key Laboratory for Carbon-Based Functional Materials & Devices, Soochow University, 199 Ren'ai Rd, Suzhou 215123, Jiangsu, P. R. China. E-mail: jliu@suda.edu.cn

b. University of Groningen and University Medical Center Groningen, Department of Biomedical Engineering, Antonius Deusinglaan 1, 9713 AV Groningen, The Netherlands. E-mail: r.shi@umcg.nl

c. Department of Dental Materials, Shanghai Biomaterials Research & Testing Center, Shanghai Ninth People's Hospital, Shanghai Jiao Tong University School of Medicine; College of Stomatology, Shanghai Jiao Tong University; National Center for Stomatology; National Clinical Research Center for Oral Diseases; Shanghai Key Laboratory of Stomatology, Shanghai, 200011, P.R. China.

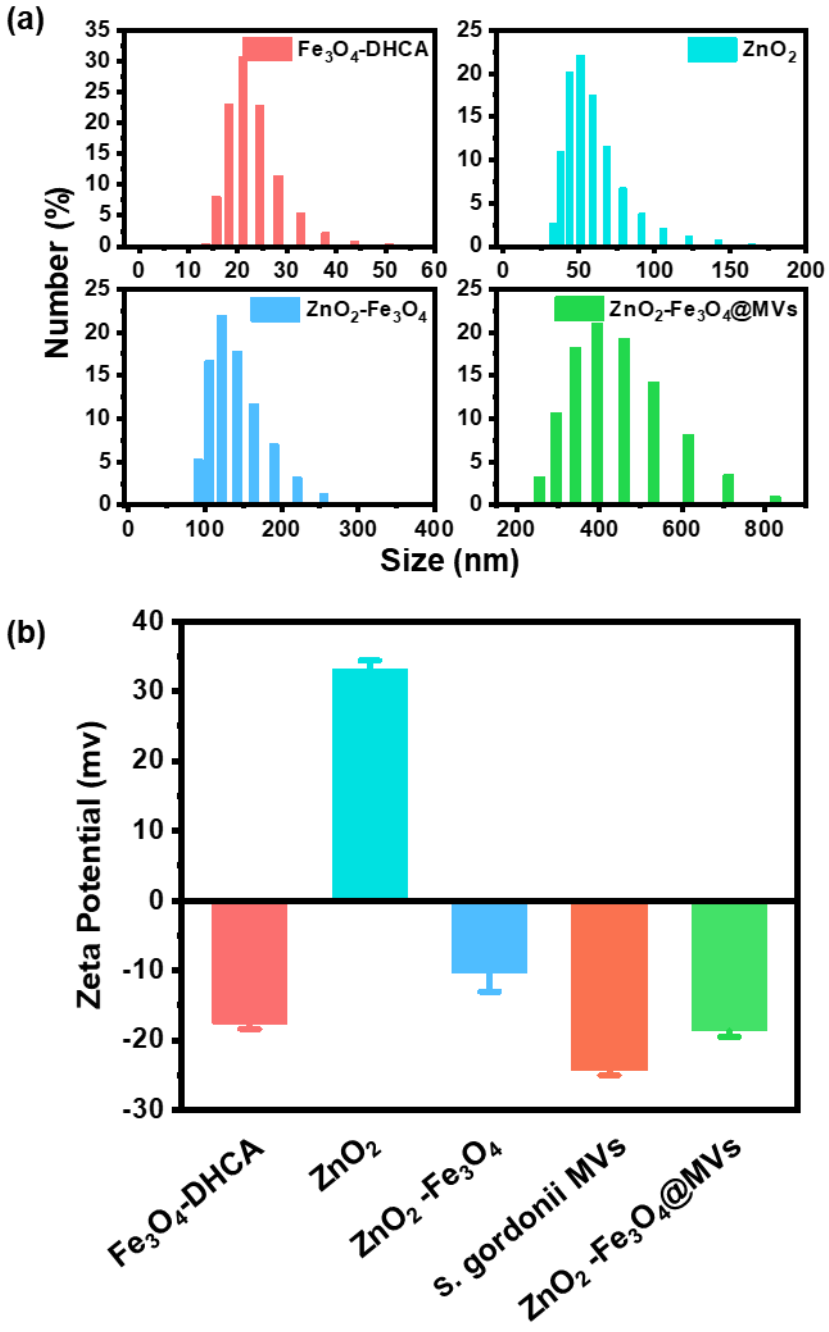

Fig. S1. DLS and zeta potential characterization of each part of the materials. (a) DLS characterization of Fe_3O_4-DHCA NPs, ZnO_2 NPs, ZnO_2–Fe_3O_4 NPs and ZnO_2–Fe_3O_4@MV NPs dispersed in water. (b) Surface zeta potentials of Fe_3O_4-DHCA NPs, ZnO_2 NPs, ZnO_2–Fe_3O_4 NPs, *S. gordonii* MVs and ZnO_2–Fe_3O_4@MV NPs. Error bar: standard deviation (n = 3).

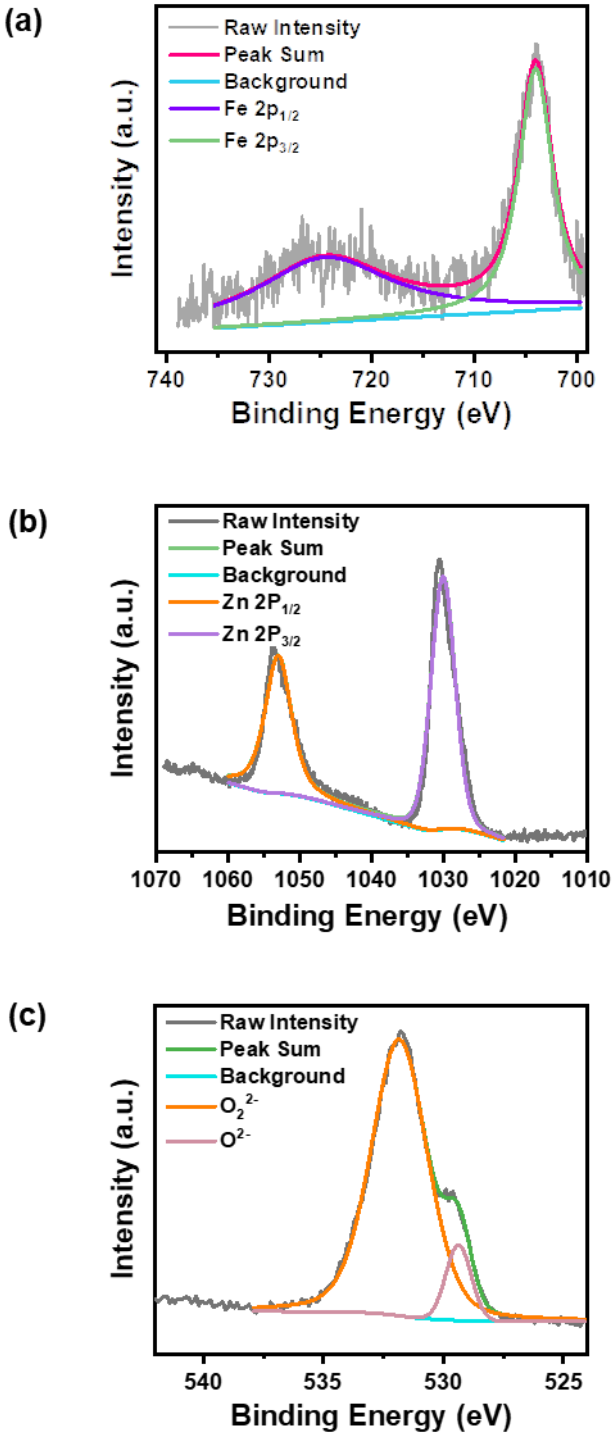

Fig. S2. X-ray photoelectron spectroscopy characterization of ZnO_2–Fe_3O_4@MV NPs. XPS spectra of Fe 2p (a), Zn 2p (b) and O 1 s (c) for ZnO_2–Fe_3O_4@MV NPs.

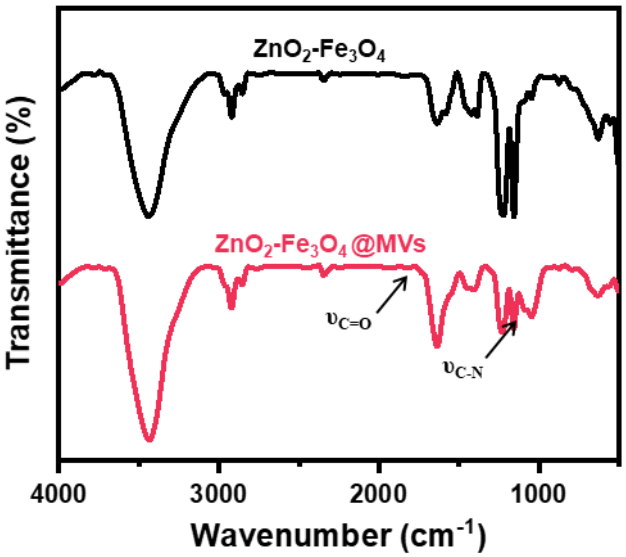

Fig. S3. Fourier-transform infrared spectroscopy characterization. FT-IR spectra of ZnO_2–Fe_3O_4 NPs and ZnO_2–Fe_3O_4@MV NPs, respectively.

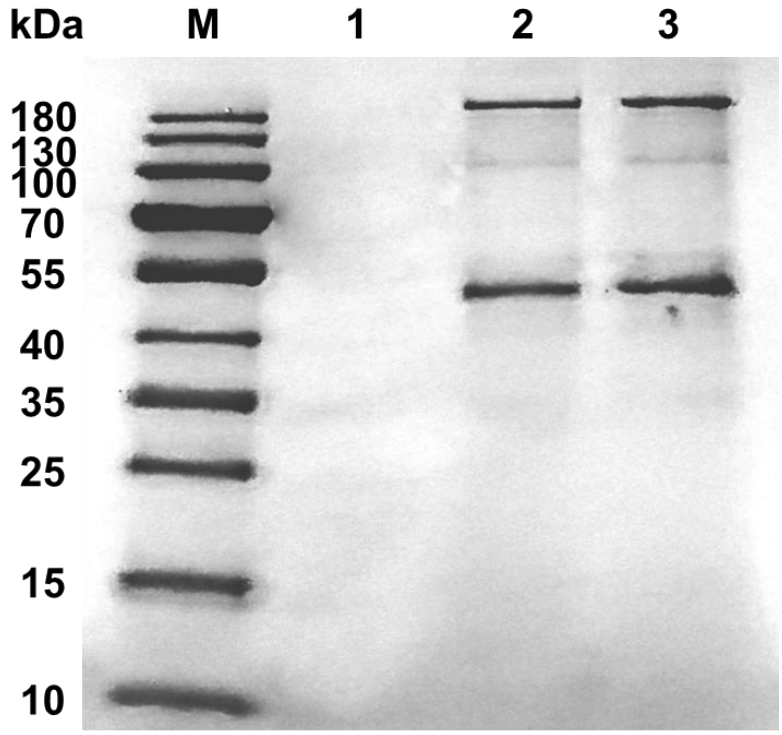

Fig. S4. Protein bands of *S. gordonii* MVs by Coomassie brilliant blue staining.
Lane M: Prestained marker
Lane 1: ZnO_2–Fe_3O_4 NPs
Lane 2: *S. gordonii* MVs
Lane 3: ZnO_2–Fe_3O_4@MV NPs

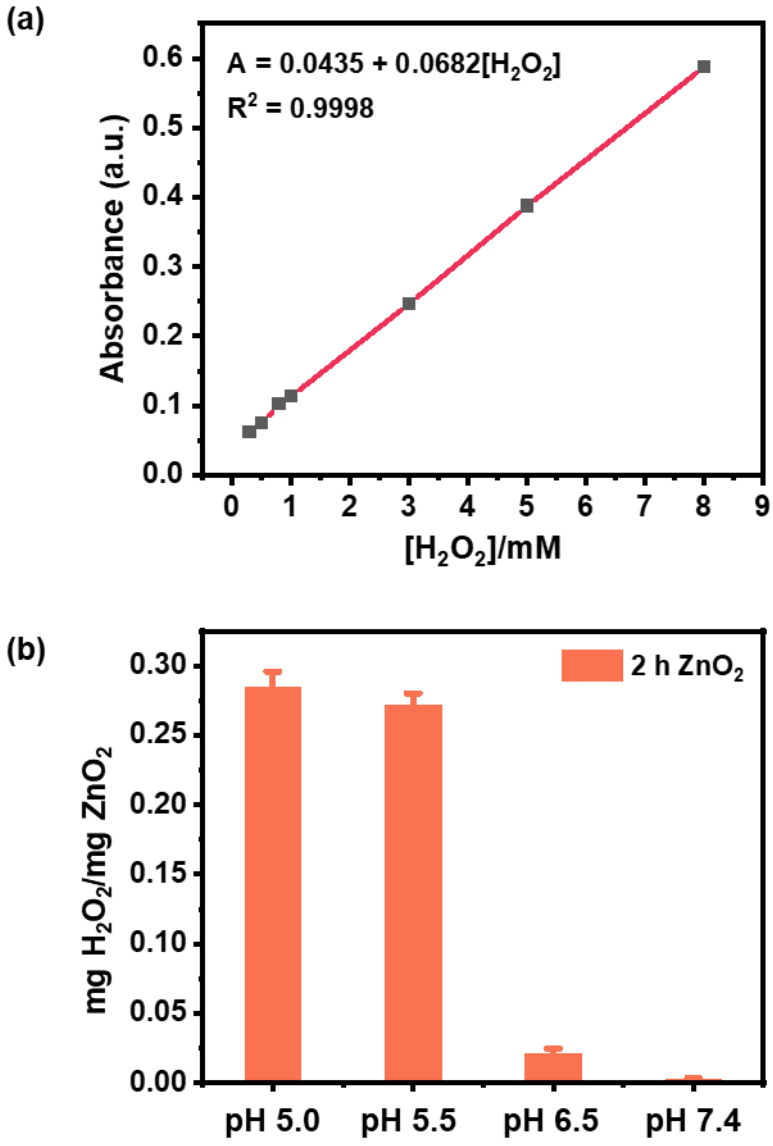

Fig. S5. Measurements of H_2O_2 production by ZnO_2 with Hydrogen Peroxide Content Assay Kit (a) Quantification of H_2O_2 in ZnO_2 NPs. (b) The ratios of the amount of H_2O_2 produced to the mass of ZnO_2 at different pH values. Error bar: standard deviation (n = 3).

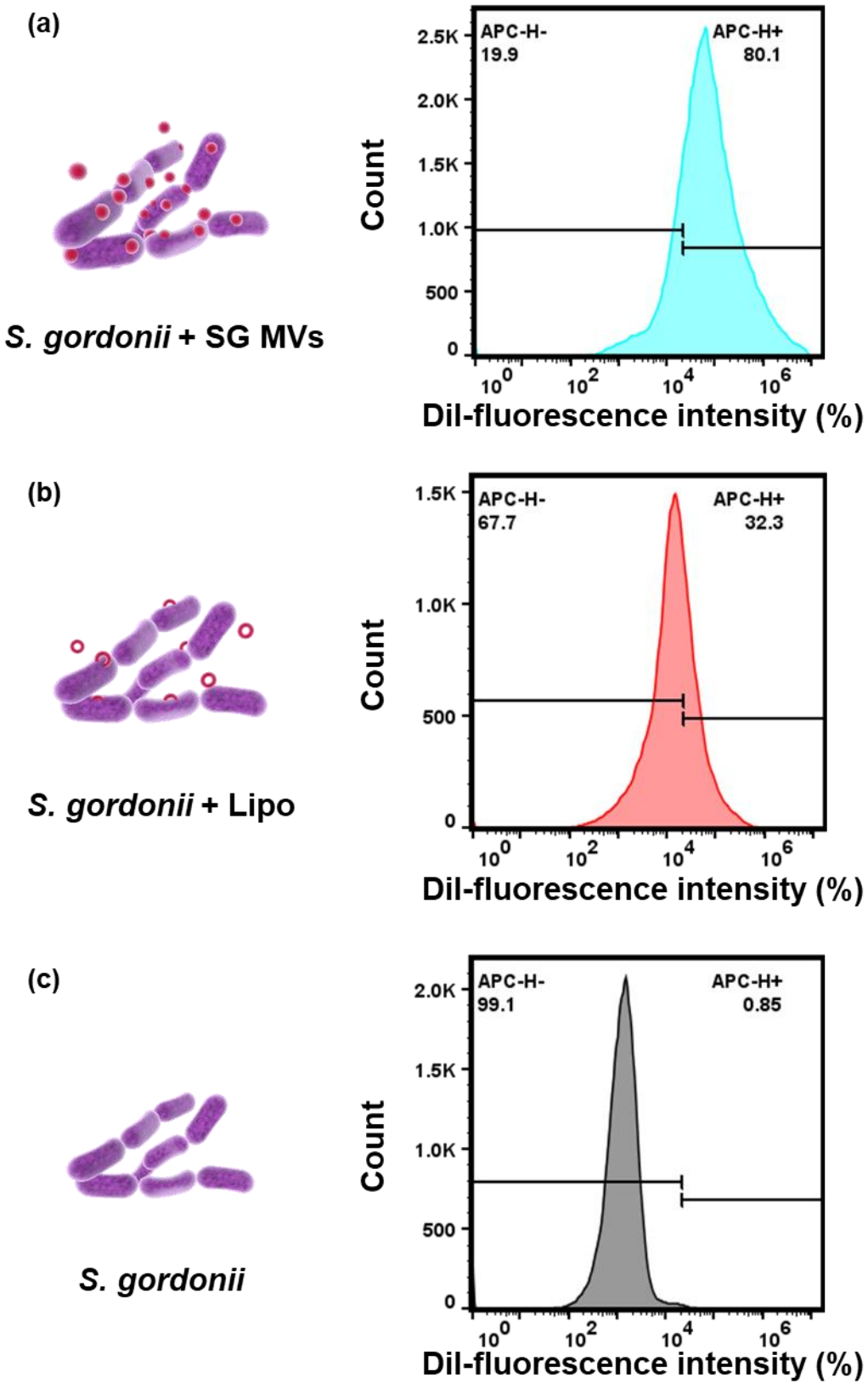

Fig. S6. Flow cytometry analysis of the uptake by individual bacteria of DiI-loaded SG MVs from parental *S. gordonii*. Lipo@DiI and PBS were used as control. Flow cytometry counts as a function of the red-fluorescence intensity due to SG MVs and Lipo@DiI uptake by *S. gordonii*.

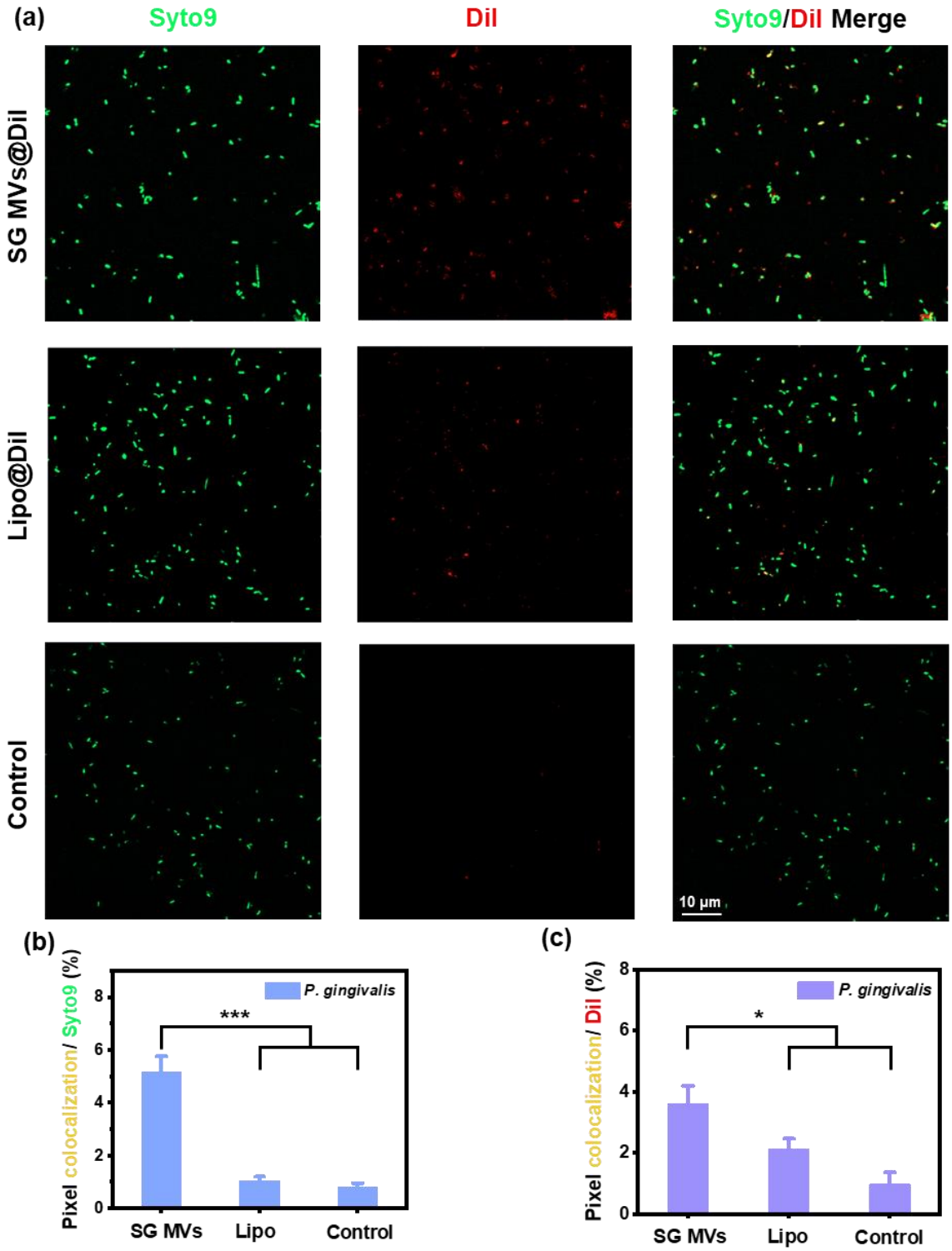

Fig. S7. Confocal fluorescence images of *P. gingivalis* incubated with *S. gordonii* MVs and image analysis. (a) Confocal fluorescence images of *P. gingivalis* incubated with SG MVs@DiI, Lipo@DiI, and PBS control for 2 h. Green fluorescence: *P. gingivalis* stained by Syto9, E_m: 488 nm; Red fluorescence: *S. gordonii* MVs and liposomes stained by DiI, E_m: 565 nm. Yellow: merge of the green and the red. Scale bar: 10 μm. (b) The area ratios of colocalized pixels of both the green and the red normalized by the pixels of the green (Syto9). (c) The area ratios of colocalized pixels of both the green and the red normalized by the pixels of the red (DiI). Error bar: standard deviation (n = 3). Statistical significance by one-way analysis of variance (*p < 0.05, ***p < 0.001).

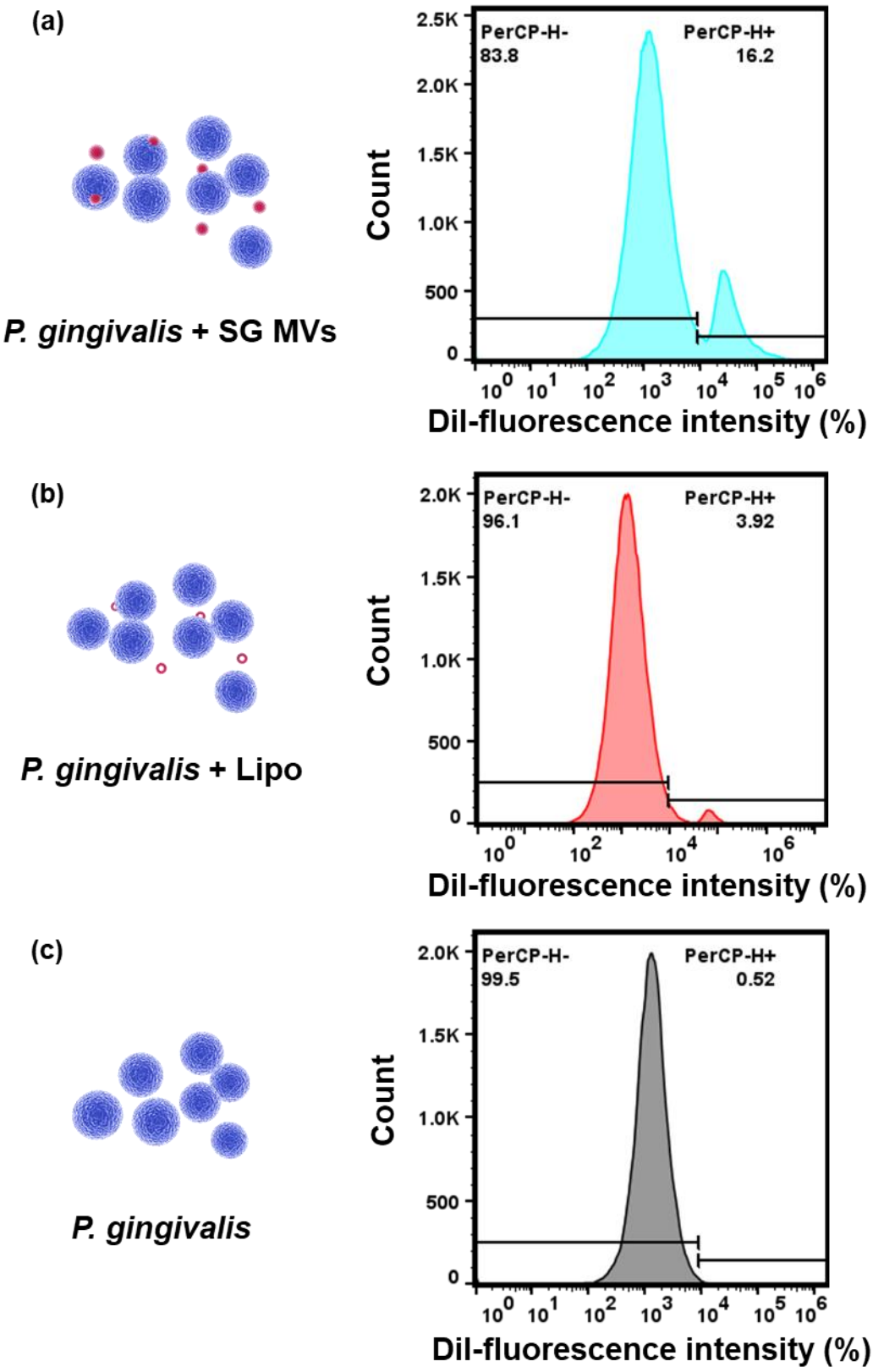

Fig. S8. Flow cytometry analysis of the uptake by individual bacteria of DiI-loaded SG MVs from *P. gingivalis*. Lipo@DiI and PBS were used as control. Flow cytometry counts as a function of the red-fluorescence intensity due to SG MVs and Lipo@DiI uptake by *P. gingivalis*.

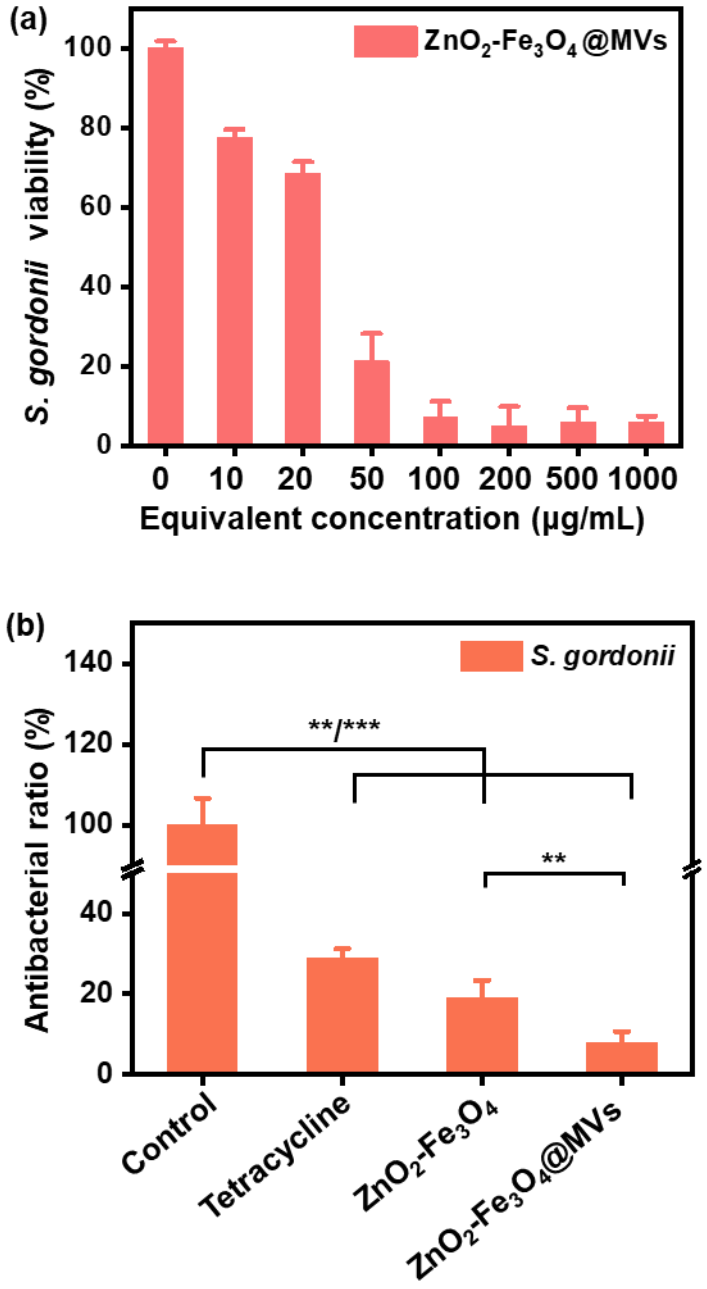

Fig. S9. Bacterial viability evaluation by colony counting after (a) the treatment of ZnO_2-Fe_3O_4@MV NPs at different concentrations; and (b) different treatments including PBS, tetracycline, ZnO_2-Fe_3O_4 NPs and ZnO_2-Fe_3O_4@MV NPs. Error bar: standard deviation (n = 3). Statistical significance by one-way analysis of variance (**p < 0.01, ***p < 0.001).

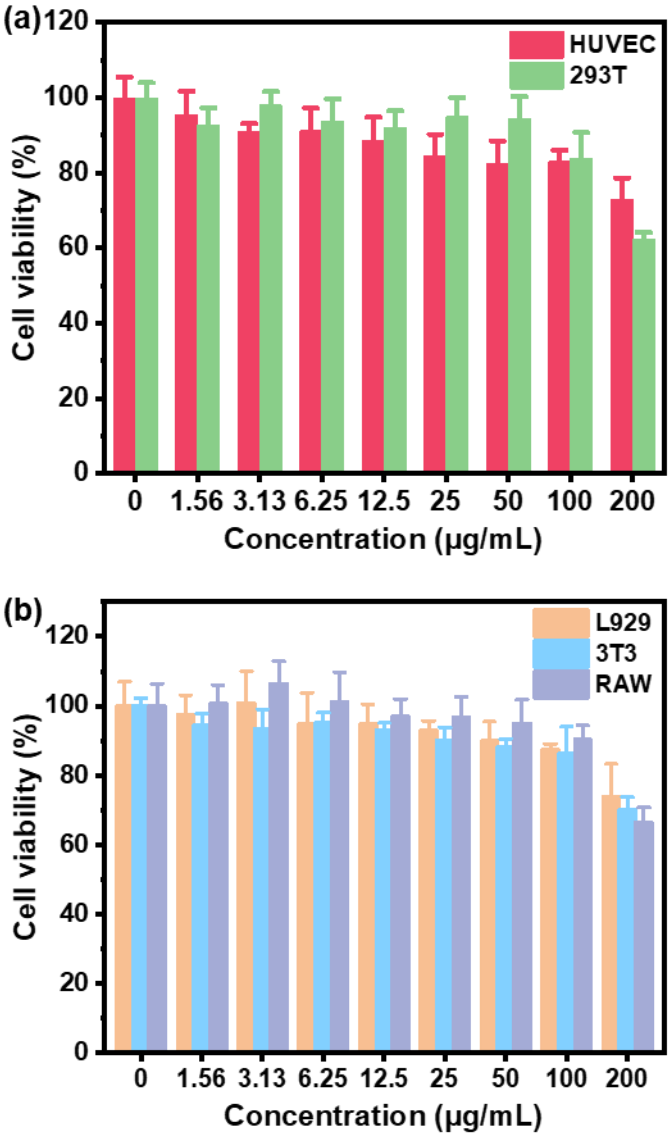

Fig. S10. Biocompatibility assessment of ZnO_2-Fe_3O_4@MV NPs. (a) Human derived cell viability evaluation by ZnO_2-Fe_3O_4@MV NPs, including 293T cells and HUVECs cells. (b) The evaluation of the biocompatibility of normal mouse derived cells by ZnO_2-Fe_3O_4@MV NPs, including L929 cells, 3T3 cells and RAW 264.7 cells. Incubation: 24 h. Error bar: standard deviation (n = 3).

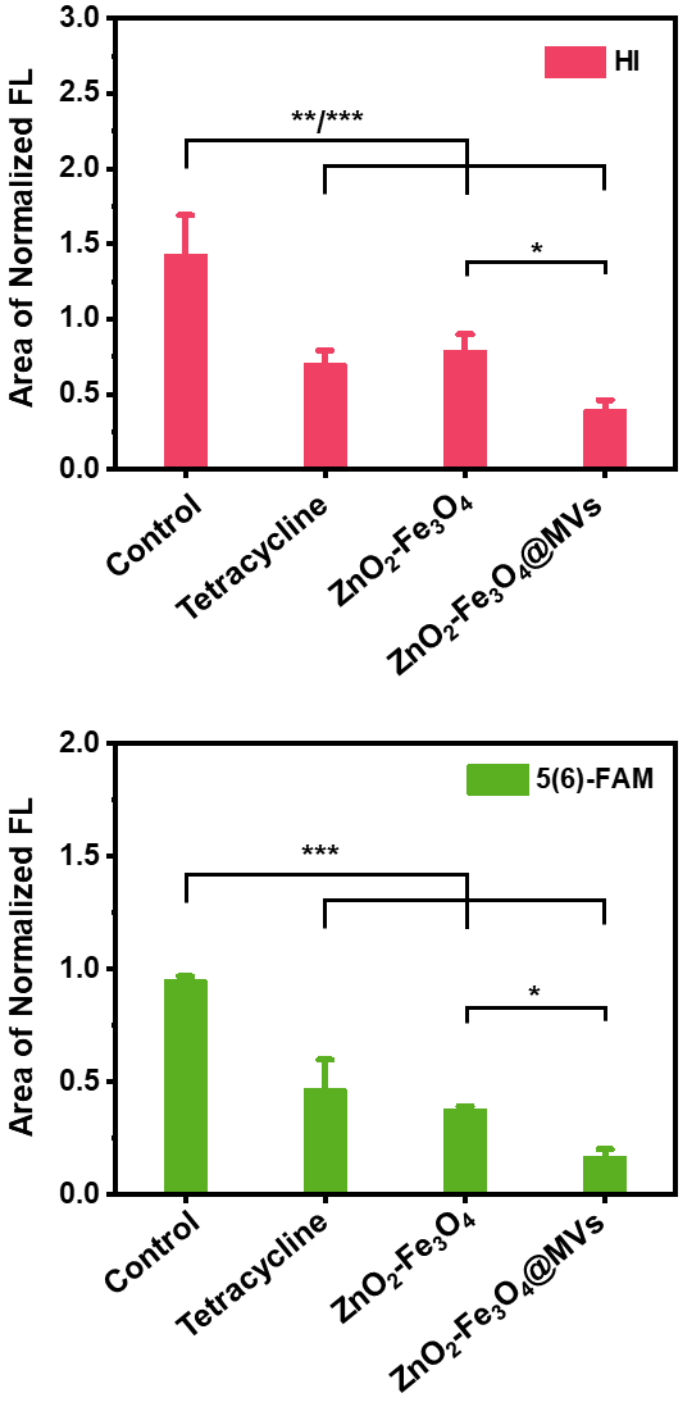

Fig. S11. Comparison of the accumulative peak areas from the curves in Fig. 4b-c. Error bar: standard deviation (n = 3). Statistical significance by one-way analysis of variance (*p < 0.05, **p < 0.01, ***p < 0.001).

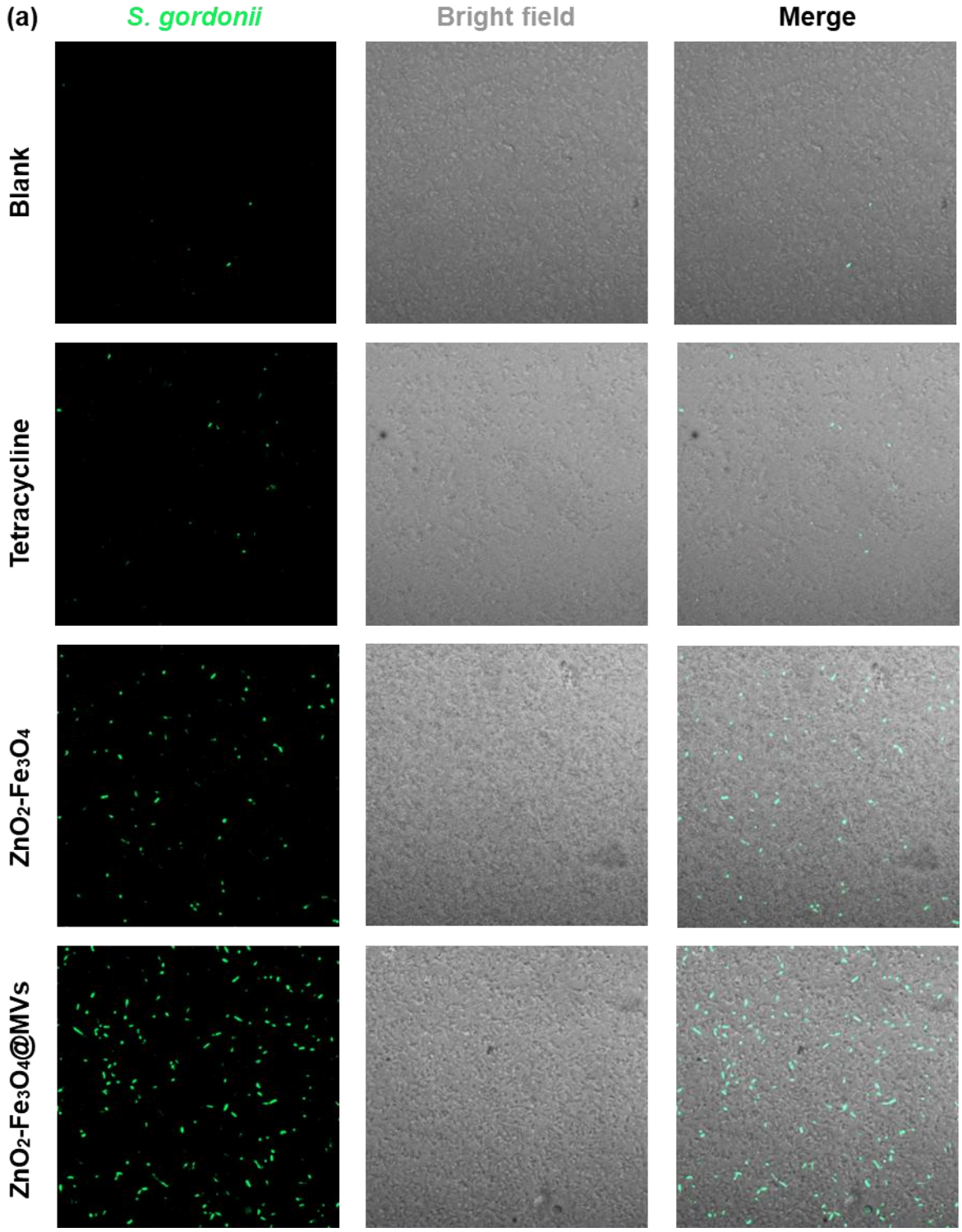
(a)
S. gordonii
Bright field
Merge
Blank
Tetracycline
ZnO2-Fe3O4
ZnO2-Fe3O4@MVs

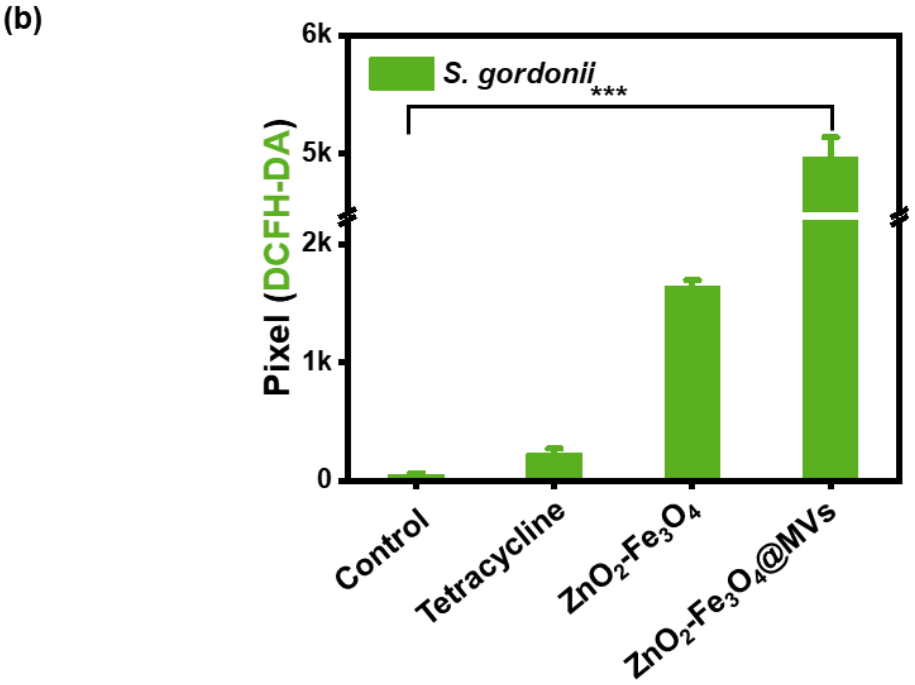

Fig. S12. Fluorescence images and analysis of ROS in planktonic bacteria (*S. gordonii*) by different treatments including PBS, tetracycline, ZnO_2-Fe_3O_4 NPs and ZnO_2-Fe_3O_4@MV NPs. (a) Fluorescence images of planktonic bacteria (*S. gordonii*). ROS probe: DCFH-DA. (b) Accumulative pixel areas of the fluorescence images at the channel of DCFH-DA. Error bar: standard deviation (n = 3).

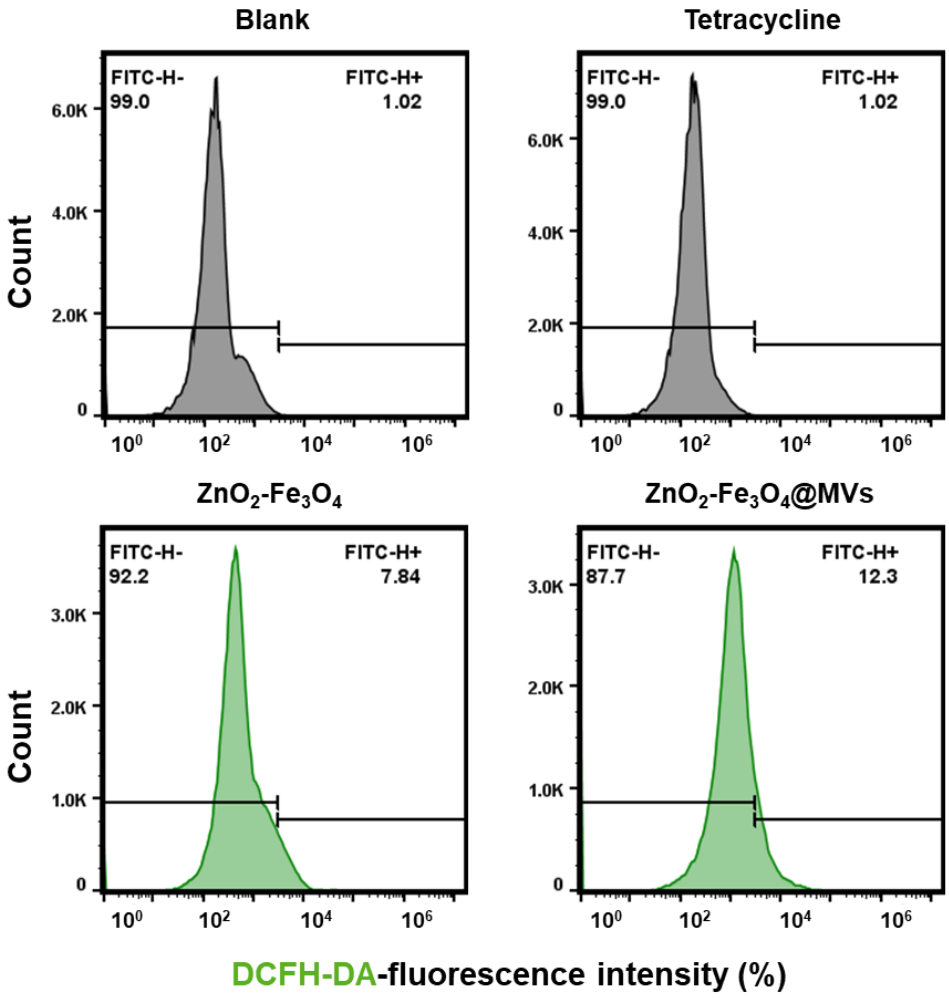

Fig. S13. Flow cytometry analysis of the uptake by ROS in planktonic bacteria (*S. gordonii*) by different treatments including PBS, tetracycline, ZnO_2-Fe_3O_4 NPs and ZnO_2-Fe_3O_4@MV NPs. ROS probe: DCFH-DA.

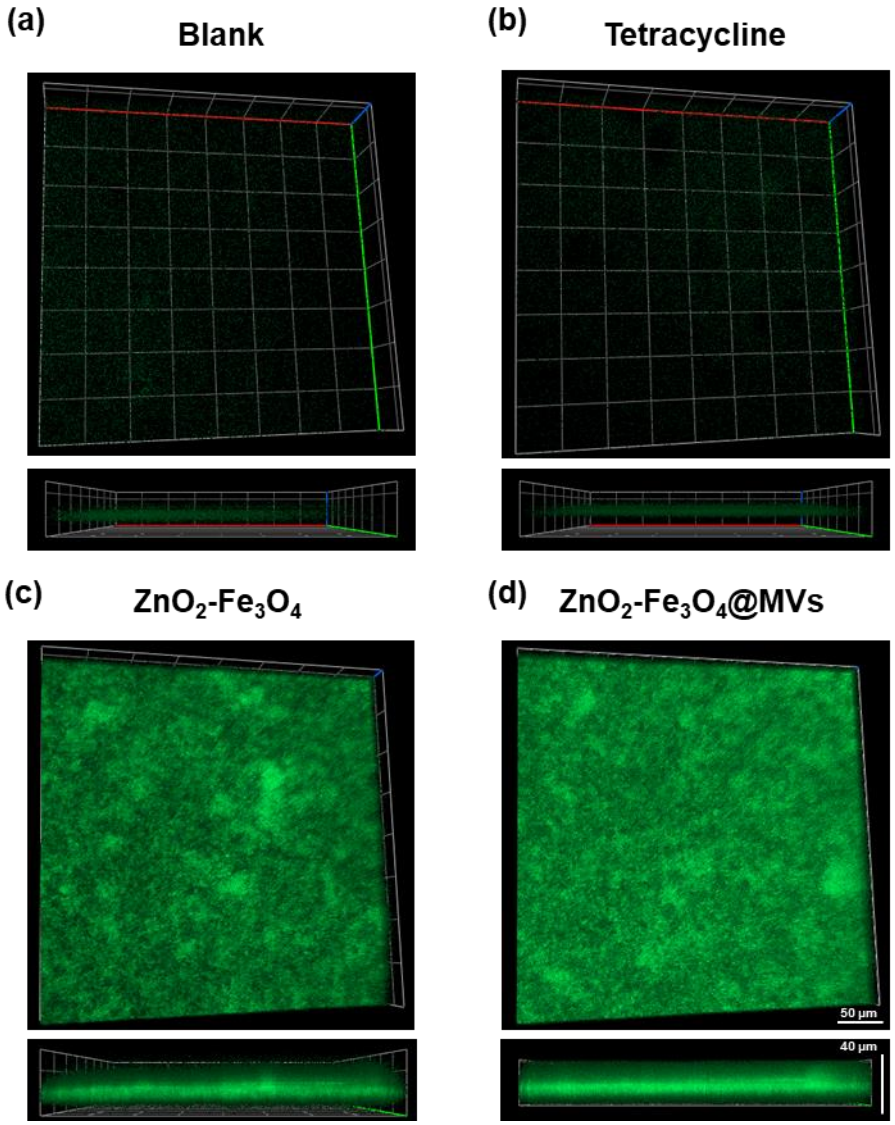

Fig. S14. Fluorescence images and analysis of ROS in symbiotic biofilms by different treatments including (a) PBS, (b) tetracycline, (c) ZnO_2-Fe_3O_4 NPs and (d) ZnO_2-Fe_3O_4@MV NPs. ROS probe: DCFH-DA.

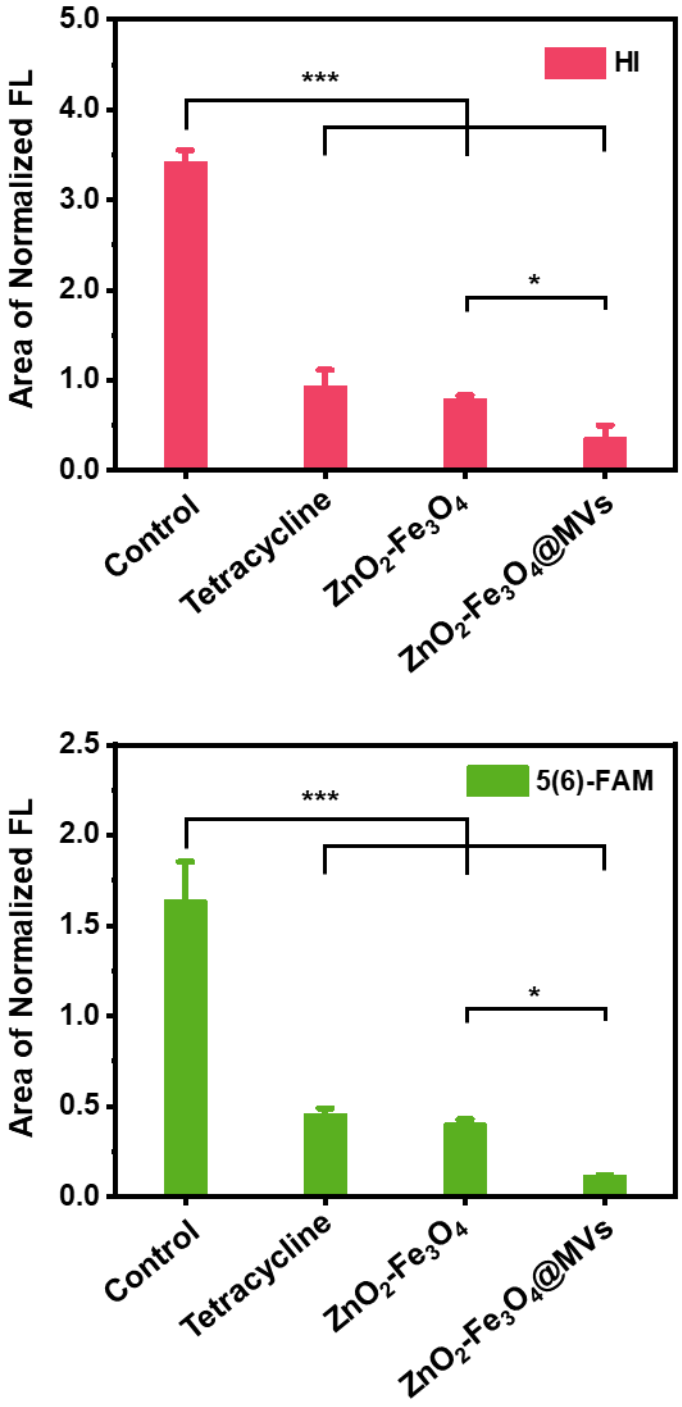

Fig. S15. Comparison of the accumulative peak areas from the curves in Fig. 5b-c. Error bar: standard deviation (n = 3). Statistical significance by one-way analysis of variance (*p < 0.05, ***p < 0.001).